Phase separation and proximity effects in itinerant ferromagnet/superconductor heterostructures

C. Martens, A. Bill, and G. Seibold

Phys. Rev. B **98**, 174513 — Published 26 November 2018

DOI: 10.1103/PhysRevB.98.174513

Phase separation and proximity effects in itinerant ferromagnet - superconductor heterostructures

C. Martens,[1] A. Bill,[2,*] and G. Seibold[1,†]

[1] *Institut Für Physik, BTU Cottbus–Senftenberg, PBox 101344, 03013 Cottbus, Germany*
[2] *Department of Physics & Astronomy, California State University Long Beach, Long Beach, CA 90840, USA*

(Dated: November 1, 2018)

Heterostructures made of itinerant ferromagnets and superconductors are studied. In contrast to most previous models, ferromagnetism is not enforced by an effective Zeeman field but induced in a correlated single-band model (CSBM) that displays itinerant ferromagnetism as a mean-field ground state. In this model superconductivity and magnetism are both calculated self-consistently. We calculate the magnitude of the magnetization, the superconducting correlations and variations of the charge density self-consistently for a superconducting-magnetic bilayer by solving the Bogoliubov-de Gennes equations on a two-dimensional lattice. We determine all three quantities as a function of the Coulomb repulsion U and the ferromagnetic exchange interaction J. The CSBM displays a variety of features not present in the Zeeman exchange model. For example, the occurrence of electronic phase separation and the competition of magnetic and superconducting orders far away from the interface.

PACS numbers: 74.45+c, 75.70.Cn, 74.78.Fk, 75.30.Cr

I. INTRODUCTION

Superconductivity and ferromagnetism were long believed to be mutually exclusive phases because in a conventional superconductor the spin part of the wavefunction is a singlet which is easily broken by the strong magnetization of the ferromagnet. However, there are situations where the coexistence is possible as in an itinerant ferromagnet where the spin-up and spin-down bands are split by an effective exchange field. Following the idea of Fulde, Ferrell, Larkin and Ovchinnikov[1] one can construct a Cooper pair which is composed of two electrons with opposite spins and momenta, but acquires a finite total momentum due to the exchange field splitting and resulting different Fermi momenta. Another possibility is the formation of 'parallel spin triplet' Cooper pairs where the associated orbital part is antisymmetric either in the exchange of the electrons position or the time coordinates, the latter being called 'odd frequency pairing'.[2]

An ideal playground to study these possibilities and many related questions are heterostructures composed of superconducting and magnetic layers. Besides their relevance for studying fundamental properties of the interplay between superconductivity and magnetism such systems have also a strong relevance for applications in spintronics due for example to the possibility of acting as spin-polarized current sources.[3]

The attractive feature of nanohybrid structures is that the two phases are spatially separated and interact solely via the proximity effect. In a S/F/S junction (S being a superconductor, F a ferromagnet) Cooper pairs tunnel through the S/F interfaces and, for a thin enough ferromagnetic layer, may realize a Josephson junction.

First studies on such systems where conducted by Buzdin and collaborators[4] who predicted for example the existence of π-junctions. Here the oscillatory behavior of the superconducting state wave function leaking into the ferromagnet may lead to a reversal of the Josephson current (the $\pi-$state) with respect to the ordinary Josephson effect (correspondingly called the $0-$state) if the thickness of the ferromagnet is chosen such that there is a sign change of the wave function on either side of the junction.

In a series of papers Bergeret, Efetov and Volkov[5] predicted that under certain conditions, such as for example the presence of magnetic domains, triplet pair correlations with a non-zero (parallel) spin projection along the quantization axis might arise, even though the Cooper pairs generated in the superconducting parts of the junction are singlets. A similar conclusion was reached in Ref. 6.

Singlet and spin-zero (antiparallel) triplet projection pairs entering a ferromagnet are subject to the pair breaking effect and are thus short-range components decaying exponentially over a few nanometers, except at every change of direction of the magnetization where they are regenerated through the cascade effect.[7,8] In contrast, non-zero spin projection triplet components are comparatively long range because unaffected by magnetism and have in fact been observed in a number of experiments (see e.g. Refs. 9–16).

The creation of such long-ranged triplet components out of a singlet superconductor requires a rotation of the magnetization which can be either realized via magnetic multilayers,[11,13] conical magnets as Ho[10,11] or Heusler alloys.[17] On the theoretical side the conditions for which a long range triplet component of the order parameter can be observed in superconductor – magnetic nanojunctions has been worked out in some detail in the diffusive regime (i.e. on the basis of Eilenberger and/or Usadel equations; see *e.g.* Refs.5, 7, 8, 18–22 and references therein) and in the clean limit within the Bogoliubov-de Gennes (BdG) approach (see *e.g.* Refs. 23–34).

More recently other sources for the generation of a long-ranged triplet component have been analyzed. In particular, it has been shown that the physical mechanism of the singlet-triplet conversion can be linked to the local SU(2) invariance of magnetized systems with spin-orbit interaction.[35]

In most of the studies of S/F junctions a strong ferromagnet is considered with a Curie temperature much larger than T_c so that the influence of superconductivity on the magnetism is negligible. However, it was suggested[5,36] that under certain conditions for a ferromagnetic film attached to a S it is favorable to be in a 'cryptoferromagnetic state',[37] i.e. a segregation of the ferromagnet into small-size domains, smaller than the superconducting coherence length.

In this paper we aim to investigate the influence of superconductivity on magnetism and the charge distribution in a S/F system in the clean limit, using the Bogoliubov-de Gennes approach. The scope of the work is to treat superconductivity and ferromagnetism on equal footing, i.e. the latter is not implemented as an effective exchange field but is described by an itinerant model with ferromagnetic exchange J between the charge carriers (cf. also Refs. 38 and 42).

Many previous studies on superconducting-ferromagnetic structures with conventional superconductors considered the BdG equations in the continuum and enforced ferromagnetism with an effective Zeeman field.[28–34] Our model is implemented on a finite lattice. Works done on discrete lattices within the BdG approach have addressed the subgap conductance at FS interfaces,[23] the spatial variation of pair correlations and magnetization inside the F for different pairing symmetry (d-wave, p-wave, etc.) in the S using extended Hubbard models,[24,39–43] or the generation of parallel spin triplets in conical magnetizations such as Holmium.[26]

Here we consider pair correlations, the magnitude of the magnetization and the density of charge carriers as a function of the exchange J and correlation term U, covering the range from soft to hard F's.

The paper is organized as follows. The next section outlines the system, model and approximations of our investigations. The resulting charge density, magnetization and order parameter profiles together with the corresponding spectral properties are discussed in Secs. III and IV. Finally, the findings are summarized in Sec. V.

II. MODEL AND FORMALISM

We consider a two-dimensional superconducting system sandwiched between two ferromagnetic layers as shown in Fig. 1. We use periodic boundary conditions along x- and y-directions so that the S system is actually connected to the same ferromagnet on the left and right. Translational invariance is assumed along the y-direction. The calculations are done at zero temperature.

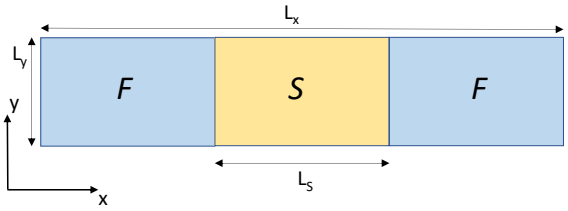

FIG. 1. Sketch of the SF bilayer proximity system with periodic boundary conditions along x- and y-directions. $L_{x,y} = N_{x,y}a$ where a denotes the lattice constant which in the following is set to $a \equiv 1$.

Our model hamiltonian reads

$$H = H_0 + H_U + H_{int}, \tag{1}$$

where

$$H_0 = \sum_{ij,\sigma} t_{ij} c^\dagger_{i,\sigma} c_{j,\sigma} + \sum_{i,\sigma} (V^{loc}_i - \mu) c^\dagger_{i,\sigma} c_{i,\sigma} + \sum_{i,\sigma} h_{i,z} \sigma c^\dagger_{i,\sigma} c_{i,\sigma} \tag{2}$$

is the single-particle part composed of the kinetic energy and a local term. The latter consists of the chemical potential μ and a local energy V^{loc}_i which is implemented in order to account for the local orbital energy but also to tune the charge density in the S layer. We consider electrons on a $N_x \times N_y$ square lattice and $c^{(\dagger)}_{i,\sigma}$ annihilates (creates) a particle with spin $\sigma = \pm 1$ at site $\mathbf{R}_i$; the site index is a two-dimensional vector, $i = (i_x, i_y)$. The hopping matrix element of the first term is set to $t_{ij} = -t < 0$ for nearest neighbors and $t_{ij} = 0$ otherwise. We also consider a constant Zeeman term $\sim h_{i,z}$ to describe the local magnetization at site i. This component of the Hamiltonian is used below to compare the results for the itinerant F system studied in this paper, with previous investigations where F was modeled with an effective exchange field $\mathbf{h}$.

The second part of Eq. (1),

$$H_U = \sum_i U_i n_{i,\uparrow} n_{i,\downarrow}, \tag{3}$$

is a local interaction with $n_{i,\sigma} = c^\dagger_{i,\sigma} c_{i,\sigma}$. Within the superconducting layers we take $U_i \equiv U_S < 0$, i.e. an attractive Hubbard interaction, in order to support singlet superconductivity. In the ferromagnetic layers U_i arises as the first term in an expansion of the long-range Coulomb interaction in Wannier functions and therefore $U_i \equiv U_F \geq 0$ in these regions.

Finally, we include a ferromagnetic exchange interaction between the electrons in the ferromagnetic layer

$$H_{int} = -\sum_{\langle ij \rangle} J_{ij} \left[\mathbf{s}_i \mathbf{s}_j + n_i n_j \right]; \quad J_{ij} > 0 \tag{4}$$

where $n_i = n_{i,\uparrow} + n_{i,\downarrow}$, $s_i^\alpha = \sum_{\sigma\sigma'} c_{i,\sigma}^\dagger \tau_{\sigma\sigma'}^\alpha c_{i,\sigma'}$ with the Pauli matrices τ^α, and $\langle ij \rangle$ limits the summations to nearest neighbor sites.

In the ferromagnetic regions ($U > 0$) our model is a particular version of a wider class of 'extended Hubbard' models which have been employed to study the occurence of ferromagnetism in a single s-band model, see e.g. Refs. 44–52, 54–58. In fact, the original motivation of the pure Hubbard model[59,60] (that considers only local interactions) was the description of band ferromagnetism which in a mean-field description occurs when the Stoner criterion $UN(E_F) > 1$ is fulfilled, where $N(E_F)$ is the density of states (DOS) at the Fermi energy. It was, however, soon realized that correlation effects strongly renormalize the Stoner condition thus suppressing the instability in most parts of the phase diagram. Extensions of the Hubbard model towards orbital degeneracy and intra-atomic Hund coupling have therefore been considered to stabilize ferromagnetism, as in Fe, Co, and Ni. However, it has been pointed in the pioneering papers by Hirsch[44–46] that also inter-site Coulomb interactions act in favor of ferromagnetism. In these papers it was shown that the interaction Eq. (4) originates from the nearest neighbor Coulomb interaction terms $J = \langle ij|1/r|ji\rangle = \langle ii|1/r|jj\rangle > 0$ obtained from the expansion of the long-range Coulomb interaction in Wannier functions.

The full expansion up to nearest neighbors contains further terms, as a standard intersite charge-charge interaction, pair hopping and correlated hopping terms. These contributions have been analyzed in e.g. Refs. 48–51, 53, 57, and 58 which in general also support ferromagnetism. Therefore, the ferromagnetic exchange term Eq. (4) plus the repulsive Hubbard interaction provide a good starting point in order to describe ferromagnetism in a single-band model. Within a slave-boson approach it has been shown[58] that in this case a ferromagnetic instability is induced for arbitrarily small exchange couplings above a critical U, in contrast to the standard Stoner model.

In the heterostructure of Fig. 1, the ferromagnetic coupling J_{ij} is only finite in the F layer. Furthermore, magnetism and charge density solely vary along the x direction and are constant along the y direction. Therefore, Eq. (4) is rewritten in the form

$$H_{int} = -\sum_{i=(i_x,i_y)} J_i^x \left[\mathbf{s}_i \mathbf{s}_{i+\hat{x}} + n_i n_{i+\hat{x}}\right] - \sum_{i=(i_x,i_y)} J_i^y \left[\mathbf{s}_i \mathbf{s}_{i+\hat{y}} + n_i n_{i+\hat{y}}\right]. \tag{5}$$

In the calculations of later sections it is assumed that $J_i^x = J_i^y = J$ is a constant within the F layer since a moderate anisotropy did not seem to affect the results significantly.

Since the system is translationally invariant along the y direction we perform the corresponding Fourier transform

$$c_{i,\sigma} = \frac{1}{\sqrt{N_y}} \sum_{i_x} c_{i_x,\sigma}(k_y) \exp(-ik_y i_y), \tag{6}$$

so that the kinetic term Eq. (2) reads ($t > 0$)

$$H_0 = -t \sum_{i_x,k_y,\sigma} \left[c_{i_x,\sigma}^\dagger(k_y) c_{i_x+1,\sigma}(k_y) + h.c.\right] + \sum_{i_x,k_y,\sigma} \left[-2t\cos(k_y) - \mu\right] c_{i_x,\sigma}^\dagger(k_y) c_{i_x,\sigma}(k_y). \tag{7}$$

We apply the transformation, Eq. (6), to the interaction terms, Eqs. (3-5). We then approximate these terms in mean-field. This includes the anomalous singlet (Gor'kov) correlations $f_0(i) = \langle c_{i,\downarrow} c_{i,\uparrow}\rangle$ that are induced in the S regions where $U_i < 0$ but leak into the F layer due to the proximity effect. In Figs. 3-8 f_0 is normalized to its bulk value f_B, obtained in absence of the adjacent F. The problem then can be diagonalized by means of the Bogoliubov-Valatin transformation

$$c_{i_x,\sigma}(k_y) = \sum_p \left[u_{i_x,\sigma}(p,k_y)\gamma_{p,k_y} - \sigma v_{i_x,\sigma}^*(p,k_y)\gamma_{p,k_y}^\dagger\right], \tag{8}$$

and the integer p labels the eigenvalue. Introducing the basis vector $\vec{\Psi}_n(p,k_y) = [u_{n,\uparrow}(p,k_y), u_{n,\downarrow}(p,k_y), v_{n,\uparrow}(p,k_y), v_{n,\downarrow}(p,k_y)]$ one has to solve the following eigenvalue problem for each value of k_y

$$\underline{\underline{H}}_{ij}(k_y)\vec{\Psi}_j(p,k_y) = \varepsilon_p(k_y)\vec{\Psi}_i(p,k_y), \tag{9}$$

where the hamiltonian is composed of a local and an intersite part

$$\underline{\underline{H}}_{i_x j_x}(k_y) = \underline{\underline{T}}_{i_x,j_x}(k_y)\left(\delta_{j_x,i_x+1} + \delta_{j_x,i_x-1}\right) + \underline{\underline{V}}_{i_x}(k_y)\delta_{j_x,i_x}. \tag{10}$$

The explicit structure of these operators is given in appendix A. The appendix also lists the mean-field decoupled densities R, Eqs. (A3)-(A10), which are calculated self-consistently. We usually start with an initial guess R_0 (usually a homogeneous superconductor and ferromagnet) and then successively calculate new densities R_n by inserting the previously obtained R_{n-1} into the mean-field hamiltonian Eq. (10) and by incorporating a weighting factor α, i.e. $R_n = \alpha R_n + (1-\alpha)R_{n-1}$. We usually set $\alpha = 0.5$ and the iteration is continued until convergence with an accuracy of $|1 - R_n/R_{n-1}| < 10^{-8}$ is reached. The procedure is repeated for different initial R_0 to search for the solution with lowest energy. We also control the stability of this lowest energy solution by checking wether the system converges to the same solution upon adding random noise to the R_n.

III. FERROMAGNETIC SYSTEM

Before presenting the results for the SF heterostructure we briefly discuss the homogeneous magnetic system, i.e.

$U_i \equiv U_F > 0$ in Eq. (3) and $J_i^x = J_i^y \equiv J$ in Eq. (5). This case is instructive for the later analysis of the competition between F and S in the interface regions. A more extensive discussion of the magnetic system can be found in Refs. 44–46, and 54. Details of the calculations are provided in appendix B.

In this work, the chosen values of parameters, U_F/t and J/t, are generic but describe realistic systems. For example, U_F is up to the order of the bandwidth, while J is typically less than U_F.[44] By investigating the Curie temperature and saturation magnetization as a function of band filling (based on a symmetric density of states) Hirsch found that a ratio of $j/(1-u) \approx 0.8$ appropriately describes ferromagnetism in Fe, Co and Ni.[44] Here, $u = UN(E_F)$ and $j = zJN(E_f)$ with z being the coordination number. Including correlated hopping Ref. 55 estimates that ferromagnetism can be found in a parameter range $0 \lesssim U/t \lesssim 1.6$ and $0.14 \lesssim J/t \lesssim 0.37$, where smaller U/t imply larger values for J/t. Note that for this estimate the single-band is associated with the e_g states of Fe with a bandwidth of ~ 2eV. Considering that correlated hopping supports ferromagnetism a parameter range $0 \lesssim U/t \lesssim 5$ and $0.2 \lesssim J/t \lesssim 0.8$ should cover the physically relevant regime for ferromagnetic metals which are explored in this paper. Note also that within the local spin density approximation the Stoner parameter $I(E_F) = UN(E_F)$ for various ferromagnetic metals has been estimated and found to increase along the third row transition metal series and decreases along the series Ni, Pd, and Pt.[61] In the mean-field approximation of the present model this parameter translates into $I(E_F) = U + Jz$ so that trends among different materials (e.g. the change of Curie temperature and magnetization) could be accessed by varying U and (or) J.

The following calculations are performed on a lattice with $N_x \times N_y = 420 \times 420$ sites. We find that the model already displays rich physics for a single magnetic layer. Depending on the parameter values the system is paramagnetic, ferromagnetic, antiferromagnetic or shows electronic phase separation.[44–46,54] To determine which of these states is stable at given values of the parameters we calculate the energy E (cf. appendix B) as a function of the spiral wave-vector $\mathbf{q}$ along the diagonal ($q_x = q_y$). The case $q = 0$ ($q = \pi$) corresponds to the ferromagnetic (antiferromagnetic) state.

In panels (a,b) of Fig. 2 we report the ground state energy $E(\mathbf{q})$ for a spiral modulation $S_i = S_0 \exp(i\mathbf{q} \cdot \mathbf{R}_i)$ as a function of $\mathbf{q}$, where S_0 is a variational parameter.

At half-filling and $U_F/t > 0$, $J/t = 0$ the system shows antiferromagnetic spin-density wave order [$\mathbf{q} = \mathbf{Q}_{AF} = (\pi, \pi)$] which due to perfect nesting occurs for infinitesimally small values of the repulsive interaction U_F/t.[62]

Upon increasing the ferromagnetic exchange $J/t > 0$ a second energy minimum develops at $\mathbf{q} = (0,0)$ which above some critical J/t that depends on U_F/t corresponds to the ferromagnetic ground state [cf. Fig. 2(a)]. As can be seen from panel (b) of Fig. 2 the same holds for doping away from half-filling where for sufficiently large

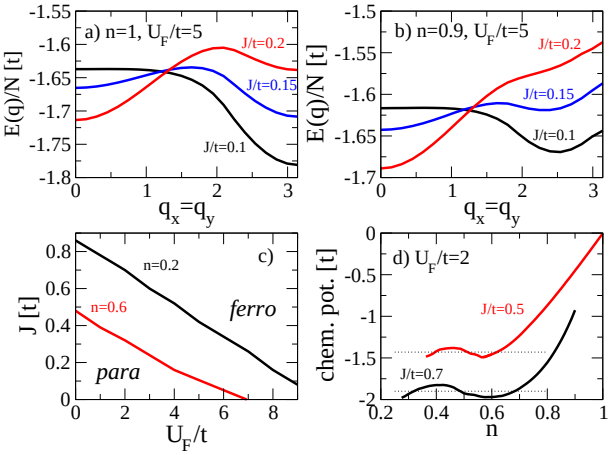

FIG. 2. Ground state energy vs. spin-spiral modulation vector $\mathbf{q}$ ($S_i = S_0 \exp(i\mathbf{q} \cdot \mathbf{R}_i)$) along the diagonal direction of the Brillouin zone at half-filling (a) and density $n = 0.9$ (b). Note that for other U_F/t results are qualitatively similar but energy variations decrease with decreasing U_F/t. (c) Phase diagram in the $(U_F/t, J/t)$-plane for density $n = 0.2$. (d) Chemical potential vs. density. The horizontal dotted lines are determined by the Maxwell construction. The compressibility diverges at the local extrema.

repulsion U_F/t and $J/t = 0$ the commensurate AF is replaced by a spiral, but with some incommensurate modulation $\mathbf{Q}_{spiral} = (q, q)$. In the regime of small doping ($n \ll 1$) and small U_F/t ($< 1/N(E_F)$) the system would be a paramagnet for $J/t = 0$ and ferromagnetism can be induced above some critical J/t. The corresponding phase diagram is displayed in Fig. (2c) for concentrations $n = 0.2$ and $n = 0.6$. Upon increasing U_F/t the transition line approaches the value for the standard Stoner criterion $U_F = 1/N(E_F)$ at $J = 0$ ($N(E_F)$ is the density of states at the Fermi energy E_F).

In Figure 2(d) we also demonstrate that the model has an instability region with respect to phase separation which can be deduced from the dependence of the chemical potential μ on the density n. The compressibility $\kappa = \partial n/\partial \mu$ diverges at the local extrema of $\mu(n)$ and becomes negative in between. The phase separation region in n is determined by the Maxwell construction (dotted horizontal line). The two curves in Fig. 2d indicate that the phase separation region decreases with decreasing J/t. Note that the occurrence of phase separation is *not* a peculiar feature of the present model. This phenomenon also appears in double exchange models that are for example used for the description of magnetism in manganites (cf. Ref. 63 and references therein).

IV. SUPERCONDUCTING-MAGNETIC HETEROSTRUCTURE

The results of this section have been obtained on lattices with 120×80 sites and periodic boundary conditions in both directions. In the S region ($40 \leq i_x \leq 80$) singlet superconductivity is generated with a negative $U_S = -2t$. For this value the coherence length can be estimated as $\xi_S \approx 4$ in units of the lattice spacing, i.e. much smaller than the linear size of the system.

The remaining sites pertain to the F region with local onsite repulsion $U_F > 0$ and ferromagnetic exchange interactions $J_i^x \equiv J^x$, $J_i^y \equiv J^y$ and $J^x = J^y = J$. This description of the F layer will be referred to as the correlated single-band model (CSBM). For comparison, we also use an effective Zeeman field h_z to model the F. The latter is referred to as the effective field model (EFM).

Since we consider an itinerant F we treat superconductivity and magnetism on equal footing. Hence, we present in this section results for the charge density, the magnetization and pair correlations in both the F and the S.

In addition to the normal proximity effect, two distinct phenomena appear in these hybrid structures: the inverse proximity effect and phase separation. In the first, the S correlations suppress the magnetization inside the F near the SF interface. In general, $n_i \neq m_i$ in such situation; the F is nowhere fully polarized. Moreover, the coupling between magnetic and charge degrees of freedom leads to a concomitant reduction of n near the SF interface. By contrast, when the system undergoes phase separation, the system is fully polarized ($n_i = m_i$) deep in the F and the superconducting state is affected by the itinerant electrons of the F.

1. *Charge density, magnetization and pair correlations*

Figure 3 reports the charge density n (panel a), magnetization m (panel b), and singlet pair correlations f_0 (panel c) in the heterostructure for varying exchange constant J/t. Since this parameter also influences the local Hartree-potential in the F layers a change of J alters the charge distribution between the S and F regions. To be able to compare results for different values of J we therefore adjust the local potential V^{loc} in the S regions in such a way that the charge density is the same for all J/t-values deep inside the S layer; hence, in panel (a) of Fig. 3 the charge densities n overlap in S for all J/t. Since most of the physics occurs close to the interface between the S and the F layer, Fig. 4 zooms into this region to show the behavior of n_i, m_i and $f_0(i)$. In addition, the figure also reports the result for the EFM (dashed lines) for $h_{i,z} = 3t$. The value of h_z is fixed in such a way that it reproduces the same magnitude of the magnetization as the CSBM deep inside the F region for $J/t = 0.5$.

From Figs. 3 and 4 one can distinguish three different regimes. For the parameters of the system, these are

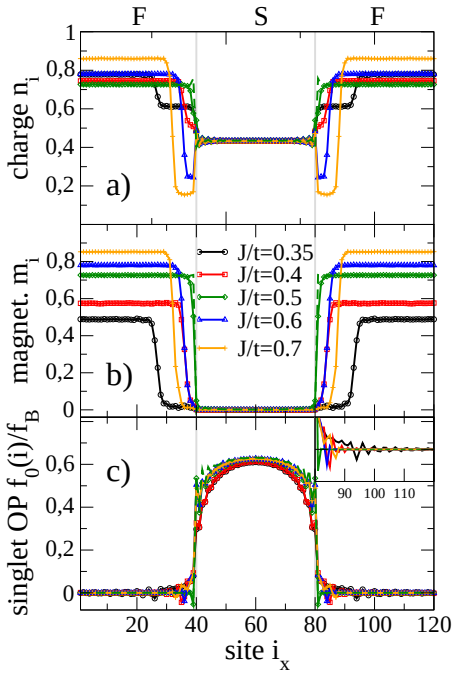

FIG. 3. Charge density (a), magnetization (b) and singlet pair correlations (c) as a function of x and various values of the exchange coupling J/t in the ferromagnetic region. For all cases the local potential V^{loc} is adjusted in such a way as to obtain a similar charge density deep in the S layer. The thin dashed green line reports the result within the EFM for $h_{i,z}/t = 3$ (see text). Parameters: $U_F/t = 2$, $U_S/t = -2$, $n = 0.625$, $f_B \approx 0.1$ is the bulk value of f_0.

$J/t \lesssim 0.3$, $0.3 \lesssim J/t \lesssim 0.55$ and $J/t \gtrsim 0.55$. At low J/t ($\lesssim 0.3$) ferromagnetism disappears; this paramagnetic regime was discussed in the previous section. Above this transition the *inverse proximity effect* regime [black open circles and red squares in panels (a-d) of Fig. 4] is effective. The S correlations completely suppress the magnetization in F over a significant distance from the interface. This regime is also characterized by a partial depletion of charge density over similar depth in the F, resulting from the coupling between charge and spin. The third regime is the *phase separation regime* found at high values of $J/t \gtrsim 0.55$ (blue triangles and gold stars). Phase separation was found in the homogeneous system of Sec. III [see Fig. 2(d)]. It is characterized by full polarization deep in the F (*i.e.* $n_i = m_i$) and a concomitant depletion of the charge density and the magnetization in the F over moderate distance away from the interface.

We note that for intermediate values, $J/t \approx 0.5$ (green diamonds), the charge and magnetic profiles adjust to reach equal value already within the charge/spin correlation length $\sim 1/k_F$ ($\approx 2-3$ lattice constants) from

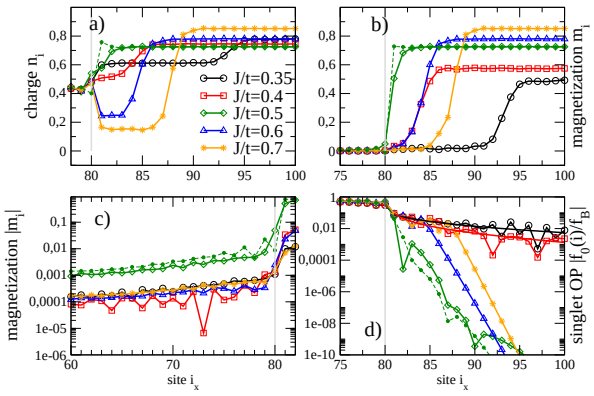

FIG. 4. Close look near the interface of the charge density (a), magnetization (b,c) and singlet pair correlations (d) shown in Fig. 3 for various values of the exchange coupling J/t in the F. For all cases the local potential V^{loc} is adjusted as described in Fig. 3. Shown for comparison as a thin dashed green line is also the pair correlation in the EFM for $h_{i,z}/t = 3$. The S correlations inside the F in panel d have been fitted with Eq. (11) (light red and black lines; see text for fitting parameters). Parameters: $U_F/t = 2$, $U_S/t = -2$, $n = 0.625$, $f_B \approx 0.1$.

the SF interface. This steep rise is close to the result of the conventional EFM (dashed green line in Figs. 3,4), where the transition is driven by the abrupt onset of the magnetization inside the ferromagnetic layer.

Figure 4(c) reveals the behavior of the magnetization in the S. The magnetization decays exponentially with a correlation length (naturally) independent of J/t. The overall magnitude is determined by the value of m_i at the interface, which is largest for intermediate values of J/t, where m_i is not suppressed by S correlations and phase separation is not relevant (diamond green lines in Fig. 4).

Figs. 3c and 4d display the decay of the superconducting order parameter $f_0(i_x)$ in the F. Panel 3(c) shows the overall behavior of the singlet order parameter for the same range of J/t values while the decay inside the F is detailed in the inset, and in panel (d) of Fig. 4 on a logarithmic scale. The latter figure shows the stark contrast between the inverse proximity ($J/t \lesssim 0.55$) and the phase separated ($J/t > 0.55$) regimes. Both cases can be modeled by the following expression

$$f_0 \sim \frac{e^{(-i_x/\xi_N)}}{i_x} \cos\left(\frac{i_x}{\xi_F}\right), \qquad (11)$$

where $\xi_N = v_F/2\pi T$ and $\xi_F = v_F/2\pi m(i_x)$ are the paramagnetic and ferromagnetic coherence lengths. A close look at the curves in Fig. 4 shows that the magnetization takes non-zero values from the interface on; for example, for $J/t = 0.35$ the value of $m(i_x)$ is small but finite already for $80 < i_x \leq 91$. The above expression for f_0, Eq. (11), can be used to obtain an excellent piecewise fit of the numerical data; one divides the space into $i_x < x_0$ and $i_x > x_0$ with $x_0 \sim 82$ ($x_0 \sim 90$) for $J/t = 0.35$ ($J/t = 0.4$). For $J/t = 0.35$ for example, the curve in regions $80 < i_x \leq x_0$ can be fitted with $\xi_N > L_F$ and $\xi_F = 30$, whereas for $i_x > x_0$ we have $\xi_N = 33$ but $\xi_F = 0.6$. For $i_x < x_0$ the pair correlation undergoes a smooth exponential decay that is expected of a paramagnet (the magnitude of $m(i_x)$ is very small in this region), whereas farther away the behavior is characteristic of a homogeneous ferromagnet. These results are consistent with previous findings for singlet pair correlations in the EFM, in a paramagnet (Ref. 27) and a homogeneous ferromagnet (see for example Ref. 4). Refs. 28 and 29 provided a complementary analysis of the decay of f_0 within the EFM. Two almost identical length scales were introduced that inversely scale with the polarization of the F and are $\sim (k_{F,\uparrow} - k_{F,\downarrow})^{-1}$. The oscillatory behavior is due to the interference of up- and down excitations in the pair amplitude.

In the opposite case of large exchange coupling J/t (phase separation regime) the pair correlations first follow the small-J/t behavior up to some distance x_0 away from the interface, followed by a much stronger decay deeper inside the F ($i_x > x_0$). The length x_0 is determined by the point where the magnetization reaches full polarization and therefore increases with J/t due to the increasing low density domain inside the F.

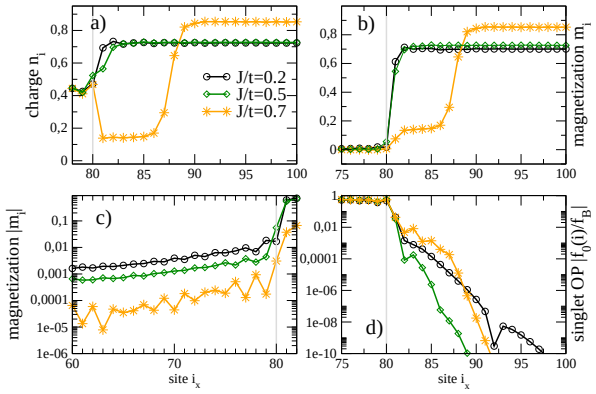

FIG. 5. Charge density (a), magnetization (b,c) and singlet pair correlations (d) close to the interface as in Figs. 3,4 but for a larger value of the Coulomb potential in the F, $U_F/t = 5$. The phase separation regime is substantially extended when compared to Figs. 3, 4. Both pair correlations in the F and the charge and magnetic configurations in S are rapidly suppressed away from the interface. Parameters: $U_F/t = 5$, $U_S/t = -2$, $n = 0.625$, $f_B \approx 0.1$.

The results of Figs. 3, 4 were obtained for $U_F/t = 2$. A larger local correlation stabilizes the F and increases the range of values of J/t for which the F is fully polarized (see Fig. 5). As a result, even for values of $J/t \approx 0.2$

close to the onset of ferromagnetism, pair correlations are not able to significantly suppress magnetism; the inverse proximity effect is almost absent. Nevertheless, this reduction of the intermediate regime does not imply a corresponding extension of the phase separation regime to lower values of J/t. At $J/t \sim 0.5$ one still observes a behavior similar to the EFM. The phase separation instability for large $J/t \gtrsim 0.5$ persists and the pair amplitude decay is again shifted away from the interface (panel (d) of Fig. 5). The distance from the interface over which the magnetization is suppressed is about the same than observed in Fig. 4. As expected, the behavior of the magnetization in the S is unaffected by the change in U_F/t in the F.

2. *Spectral properties and pair correlations*

The proximity effect is also reflected in spectral properties such as the local density of states (LDOS),

$$\rho^{loc}(i_x,\omega) = \frac{1}{N}\sum_{p,k_y,\sigma}\left[|u_{i_x,\sigma}(p,k_y)|\delta(\omega-\varepsilon_p(k_y)) - |v_{i_x,\sigma}(p,k_y)|\delta(\omega+\varepsilon_p(k_y))\right],$$

which within the BdG formalism and the EFM has been analyzed in Refs. 28 and 29.

Fig. 6 shows the LDOS deep in the S and the F. Noticeable are the standard BCS coherence peaks at the gap edges in the S (near $\omega = 0$, black curve at $i_x = 60$); a small numerical 'pair-breaking parameter' $\epsilon = 0.02t$ has been introduced for numerical reasons which is responsible for the small finite LDOS inside the gap. The overall structure of the LDOS is otherwise characteristic of a two-dimensional square lattice with its logarithmic van-Hove singularity at the band center.

Deep inside the ferromagnet [red curve at $i_x = 110$ in Fig. 6] the van Hove singularity is split due to the formation of subbands (peaks near $\omega/t \approx -1, +3$). Note that the apparent "noise" in the data is not due to the lack of precision of the calculation, but are oscillations originating from the discreteness of the lattice.

It is instructive to investigate the dynamical singlet pair correlations (Gor'kov function)

$$f_0(i_x,t) = \frac{1}{2}\left[\langle c_{ix,\uparrow}(t)c_{ix,\downarrow}(0)\rangle - \langle c_{ix,\downarrow}(t)c_{ix,\uparrow}(0)\rangle\right] \quad (12)$$

inside the ferromagnet for different exchange parameters J/t. The imaginary part of the Fourier transform reads

$$\begin{aligned} F(i_x,\omega) &= \mathrm{Im}\int_{-\infty}^{\infty} dt\ \mathrm{e}^{i\omega t} f_0(i_x,t) \quad (13)\\ &= \pi\sum_{p,k_y}\left[u_{i,\uparrow}(p,k_y)v^*_{i,\downarrow}(p,k_y) + u_{i,\downarrow}(p,k_y)v^*_{i,\uparrow}(p,k_y)\right]\\ &\times\langle\gamma_{p,k_y}\gamma^\dagger_{p,k_y}\rangle\delta(\omega+\varepsilon_p(k_y))\\ &-\pi\sum_{p,k_y}\left[u_{i,\uparrow}(p,k_y)v^*_{i,\downarrow}(p,k_y) + u_{i,\downarrow}(p,k_y)v^*_{i,\uparrow}(p,k_y)\right]\\ &\times\langle\gamma^\dagger_{p,k_y}\gamma_{p,k_y}\rangle\delta(\omega-\varepsilon_p(k_y)). \end{aligned}$$

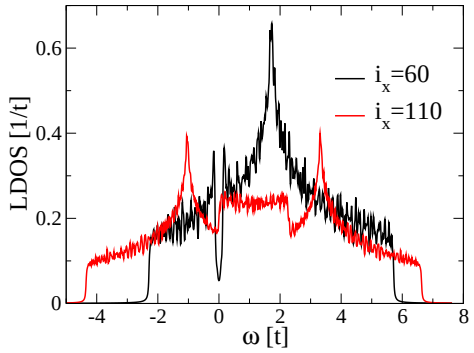

FIG. 6. Local density of states (a) inside the S (black; $i_x = 60$) and the F (red; $i_x = 110$) for $J/t = 0.5$. Other parameters: $U_F/t = 2$, $U_S/t = -2$, $n = 0.625$.

Figure 7 shows the position and frequency dependence of the singlet correlations, Eq. (13), as an intensity plot which visualizes the decay of the pair correlations inside the ferromagnet. Note that the Gor'kov functions are asymmetric in ω, $f_0(-\omega) = -f_0(\omega)$, and in a clean S system show a $\pm 1/\sqrt{\omega-\Delta}$ singularity at the gap edges [$\Delta(i_x) = |U f_0(i_x, t=0)|$ being the superconducting gap]. Only the $\omega < 0$ part of $F(i_x,\omega)$ is shown in Figs. 7 and 8 below.

A main difference between the inverse proximity regime and the phase separated regime is immediately apparent at small ω/t when comparing Figs. 7(a) and 7(b): pair correlations extend deep into the F for small J/t [Fig. 7(a)]. The region in the F where these pair correlations are present also shrinks with increasing ω/t. In the region where the magnetization is suppressed, either because of the inverse proximity effect (small J/t) or phase separation (large J/t) the low energy $F(i_x,\omega)$ continuously extends from the S region into the F. This is clearly visible in Fig. 7(a) at low ω/t where the intensity plot shows pronounced pair correlations (indicated by solid red color) close to the interface. By contrast, the Gor'kov function starts oscillating within a partially

polarized region of the ferromagnet as indicated by the alternating red-blue pattern of Fig. 7(a). Similarly, oscillations of $F(i_x,\omega)$ are seen at fixed position i_x as a function of ω/t. We now analyze this ω-dependence of $F(i_x,\omega)$ in more detail in Fig. 8 at various distances i_x from the interface in the S and the F.

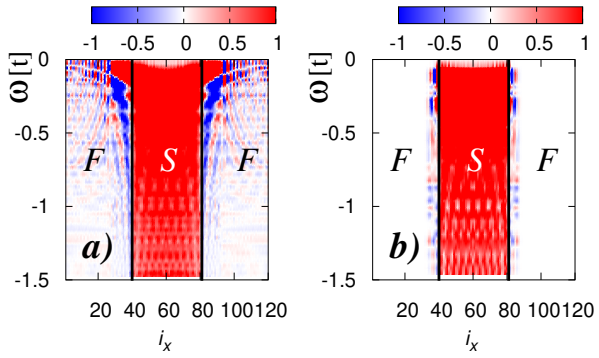

FIG. 7. Position and frequency dependent singlet correlations, Eq. (13), for (a) $J/t = 0.35$ and (b) $J/t = 0.7$. Pair correlations oscillate both in space and frequency and extend deeper into the F for small J/t. i_x indexes the site as in Fig. 3. A horizontal cut at $\omega = 0$ for these two values of J/t is shown in Fig. 3c. Vertical cuts at fixed values of i_x are shown in Fig. 8. Parameters $U_S/t = -2$, $U_F/t = 2$ $n = 0.625$, $f_B \approx 0.1$.

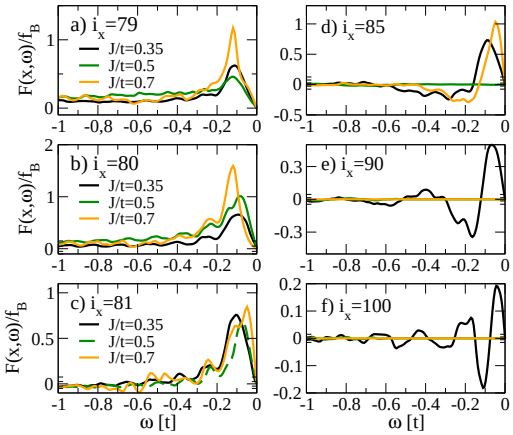

FIG. 8. Imaginary part of the singlet Gor'kov pair correlation $F(i_x,\omega)$ dependence on frequency at specific points in the heterostructure and for various exchange couplings as indicated in the panels. The correlations at $x = 79$ and $x = 80$ are in the S while those for $x \geq 81$ are in the F. Note that the singlet order parameter for $J/t = 0.5$ and $x = 81$ has opposite sign as compared to the other couplings (cf. panel (c) of Fig. 3). For better comparison we have therefore multiplied the $J/t = 0.5$ in panel (c) by -1, symbolized by the dashed line. Parameters: $U_F/t = 2$, $U_S/t = -2$, $n = 0.625$, $f_B \approx 0.1$.

The singlet pair correlations $F(i_x,\omega)$ shown in panel (a,b) of Fig. 8 are calculated at the interface, on the S side, $i_x = 79, 80$. The peak position, indicating the size of the S gap is largest (and sharpest) for $J/t = 0.7$ in agreement with the larger singlet order parameter (cf. panel (c) of Fig. 3). Interestingly, the amplitude of these pair correlations is even larger than in the bulk.

On the other side of the interface, in the F ($i_x = 81$, panel (c) of Fig. 8) one still observes a sizable gap for all couplings, which however, is now largest for $J/t = 0.35$ where the magnetization is suppressed close to the interface. Further away from the interface, at $i_x = 85$, panel (d) shows that for $J/t = 0.5$ the magnetic system is already completely polarized, and the pair correlations are suppressed on the scale of the plot. Interestingly, at this same location, the phase separated solution ($J/t = 0.7$) and the inverse proximity solution ($J/t = 0.35$) still reveal a low energy peak and thus the occurrence of a proximity induced gap. Moreover, at larger energies ($\omega/t \sim -0.3$) a second broad peak appears with opposite sign. For $J/t = 0.35$ this peak turns out to be related to the onset of frequency oscillation in $F(i_x,\omega)$ observed further away from the interface, as seen in panels (e) and (f). In the diffusive limit and within the EFM[4,5] it was shown that the occurrence of such oscillations in frequency is a direct consequence of the exchange field h. Similarly, in the BdG approach they arise from the superposition of the different excitations in the spin-up and down bands and thus disappear when the system is completely polarized. This explains why in panel (e) and (f), at $i_x = 90, 100$, only pair correlations in the inverse proximity regime ($J/t = 0.35$) are finite. Note that the frequency integration of $F(i_x,\omega)$ yields the local (equal time) Gor'kov function $f_0(i_x, t = 0)$ at i_x which vanishes in the F region and thus requires a cancellation of the finite contributions to $F(i_x,\omega)$.

Finally, we note in panels (d-f) that there are smaller oscillations, both in magnitude and frequency, superposed to the large oscillation of $F(i_x,\omega)$ just mentioned. These are the same small oscillations found in all curves of panels (b,c) and are related to the discrete spatial lattice.

The results of this section IV were obtained for singlet pair correlations generated in the S and leaking into the F. A similar behavior is also found for spin zero projected triplet correlations brought about in the F region. In the SF hybrid structure with periodic boundary conditions studied here, the magnitude of the magnetization is inhomogeneous while its orientation is fixed. Hence, there are no parallel spin projected triplet states. This contrasts the magnetic and superconducting inhomogeneities discussed here from those of previous work.[7,8,20–22]

V. CONCLUSION

We have analyzed proximity effects in a FS heterostructure in which the F is described within an extended Hubbard-type model where the ferromagnetic exchange arises from intersite contributions of the Coulomb

interaction. Such a description allows the self-consistent treatment of both superconducting and magnetic order parameters which gives rise to features not present in approaches where the exchange field is fixed inside the F. In particular, we have found that for small exchange interactions and onsite correlations the magnetization close to the interface may be suppressed by the S correlations which significantly alters the decay of the pair correlations inside the F. Similarly, for large exchange couplings the system shows an instability towards phase separation which is also realized close to the interface with a concomitant suppression of the magnetization. As a consequence the S correlations extend far inside the phase separated region and only get suppressed when the magnetization recovers at some distance from the interface. The correlations leak much deeper than for the effective field model; this may significantly affect the Josephson current and is being investigated. Such an instability towards phase separation is also inherent in double-exchange models for ferromagnetism which are usually considered to be appropriate for transition metals[63]. Therefore, we expect that these aspects of our results are also valid in such systems and are planned in future investigations. In the present paper we have restricted ourselves to collinear magnetic structures. However, microscopic magnetic models usually show also more complex magnetic structures in some part of the phase diagram, as for example the antiferromagnetic spirals in panel (b) of Fig. 2 for $J/t = 0.1$. A heterostructure where the ferromagnet displays a spiral rotation would also induce $m = 1$ triplet components inside the F. As a result, we expect that the pair correlations inside the F have a pronounced influence on the periodicity of such magnetic structures. Work in this direction is in progress.

VI. ACKNOWLEDGEMENTS

CM and GS thank the DAAD for financial support. AB gratefully acknowledges funding provided by the National Science Foundation (DMR-1309341).

Appendix A

The matrices defined in Eq. (10) are given by

$$\underline{\underline{T}}_{i,i+x}(k_y) = \begin{pmatrix} -t + 2J_i^x(k_{i,\uparrow}^x + k_{i,\downarrow}^x)^* & 0 & 0 & 2J_i^x p^x(i) \\ 0 & -t + 2J_i^x(k_{i,\uparrow}^x + k_{i,\downarrow}^x)^* & 2J_i^x p^x(i+x) & 0 \\ 0 & 2J_i^x p^x(i) & t - 2J_i^x(k_{i,\uparrow}^x + k_{i,\downarrow}^x) & 0 \\ 2J_i^x p^x(i+x) & 0 & 0 & t - 2J_i^x(k_{i,\uparrow}^x + k_{i,\downarrow}^x) \end{pmatrix}$$

and

$$\underline{\underline{V}}_{i}(k_y) = \begin{pmatrix} -2t\cos(k_y) + v_{\uparrow,\uparrow}(i) & v_{\uparrow,\downarrow}(i) & 0 & U_i f_0(i) + 2J_i^y p^y(i) \\ v_{\downarrow,\uparrow}(i) & -2t\cos(k_y) + v_{\downarrow,\downarrow}(i) & U_i f_0(i) + 2J_i^y p^y(i) & 0 \\ 0 & U_i\Delta_i^* + 2J_i^y[p^y(i)]^* & 2t\cos(k_y) - v_{\uparrow,\uparrow}(i) & v_{\uparrow,\downarrow}^*(i) \\ U_i\Delta_i^* + 2J_i^y[p^y(i)]^* & 0 & v_{\downarrow,\uparrow}^*(i) & 2t\cos(k_y) - v_{\downarrow,\downarrow}(i) \end{pmatrix}$$

with the following abbreviations

$$\begin{aligned} v_{\sigma,\sigma}(i) &= \frac{U_i}{2}(n_i - \sigma m_i) + V_i^{loc} - \mu + h_{i,z}\sigma \qquad \text{(A1)} \\ &\quad - J_{i-x}^x(n_{i-x} + \sigma m_{i-x}) - J_i^x(n_{i+x} + \sigma m_{i+x}) \\ &\quad - 2J_i^y(n_i + \sigma m_i) + 4J_i^y Re[(k_{i,\uparrow}^y + k_{i,\downarrow}^y)e^{ik_y}] \\ v_{\uparrow,\downarrow}(i) &= -U_i\langle S_i^-\rangle - 2J_{i-x}^x\langle S_{i-x}^-\rangle - 2J_i^x\langle S_{i+x}^-\rangle \\ &\quad - 4J_i^y\langle S_i^-\rangle \qquad \text{(A2)} \\ n_i &= \sum_\sigma \langle n_{i,\sigma}\rangle \qquad \text{(A3)} \\ m_i &= \sum_\sigma \sigma\langle n_{i,\sigma}\rangle \;\; (\sigma = \pm 1) \qquad \text{(A4)} \\ \Delta_i &= \langle c_{i,\downarrow}c_{i,\uparrow}\rangle \qquad \text{(A5)} \end{aligned}$$

$$\langle S_i^-\rangle = \langle c_{i,\downarrow}^\dagger c_{i,\uparrow}\rangle = \frac{1}{N_y}\sum_{k_y}\langle c_{i,\downarrow}^\dagger(k_y)c_{i,\uparrow}(k_y)\rangle \qquad \text{(A6)}$$

$$k_{i,\sigma}^x = \langle c_{i,\sigma}^\dagger c_{i+x,\sigma}\rangle = \frac{1}{N_y}\sum_{k_y}\langle c_{i,\sigma}^\dagger(k_y)c_{i+x,\sigma}(k_y)\rangle \qquad \text{(A7)}$$

$$k_{i,\sigma}^y = \langle c_{i,\sigma}^\dagger c_{i+y,\sigma}\rangle = \frac{1}{N_y}\sum_{k_y} e^{-ik_y}\langle c_{i,\sigma}^\dagger(k_y)c_{i,\sigma}(k_y)\rangle \qquad \text{(A8)}$$

$$p^x(i) = \langle c_{i,\downarrow}c_{i+x,\uparrow}\rangle = \frac{1}{N_y}\sum_{k_y}\langle c_{i,\downarrow}(k_y)c_{i+x,\uparrow}(k_y)\rangle \qquad \text{(A9)}$$

$$p^y(i) = \langle c_{i,\downarrow}c_{i+y,\uparrow}\rangle e^{-ik_y} + \langle c_{i+y,\downarrow}c_{i,\uparrow}\rangle e^{ik_y}\,. \qquad \text{(A10)}$$

Appendix B

In Sec. III we discuss the magnetic state of the F alone, in the correlated single band model, Eq. (9). Spiral magnetic solutions with the Ansatz $\langle S_i^{\pm}\rangle = S_0 \exp(\pm i\mathbf{q}\mathbf{R_i})$ are obtained by factorizing Eqs. (3, 4) with respect to the operators

$$S_q^{+(-)} = \sum_{\mathbf{k}} c^{\dagger}_{\mathbf{k}+\mathbf{q}\uparrow(\downarrow)} c_{\mathbf{k}\downarrow(\uparrow)} \, .$$

Since the charge density for these solutions is constant Hartree terms are neglected as they only shift the energy by a constant value. For a given momentum $\mathbf{q}$ the resulting energy is given by

$$E(\mathbf{q}) = \sum_{\mathbf{k}}^{N} \left\langle \begin{pmatrix} c^{\dagger}_{\mathbf{k}+\mathbf{q}\uparrow} c^{\dagger}_{\mathbf{k}\downarrow} \end{pmatrix} \underline{\underline{H}} \begin{pmatrix} c_{\mathbf{k}+\mathbf{q}\uparrow} \\ c_{\mathbf{k}\downarrow} \end{pmatrix} \right\rangle + 4JNS_0^2(cos(q_x)+cos(q_y)) - 2JN(v_x^2+v_y^2) + UNS_0^2, \tag{B1}$$

where

$$\underline{\underline{H}} = \begin{pmatrix} \varepsilon_{\mathbf{k}+\mathbf{q}} + \frac{2J}{t}\left[v_x\cos(k_x+q_x) + v_y\cos(k_y+q_y)\right] & -\frac{4JS_0}{t}\left[\cos(q_x)+\cos(q_y)\right] - \frac{US_0}{t} \\ -\frac{4JS_0}{t}\left[\cos(q_x)+\cos(q_y)\right] - \frac{US_0}{t} & \varepsilon_{\mathbf{k}} + \frac{2J}{t}\left[v_x\cos(k_x) + v_y\cos(k_y)\right] \end{pmatrix} . \tag{B2}$$

The quantities

$$v_{x/y} = \frac{1}{N}\sum_{k\sigma} \cos(k_{x/y})\langle n_{\mathbf{k}\sigma}\rangle \, .$$

renormalize the kinetic energy via the magnetic interaction and have to be determined self-consistently.

* andreas.bill@csulb.edu
† goetz.seibold@tu-cottbus.de

[1] P. Fulde and R. A. Ferrell, Phys. Rev. **135**, A550 (1964); A. I. Larkin and Y. N. Ovchinnikov, Sov. Phys. JETP **20**, 762 (1965).
[2] V. L. Berezinskii, JETP Lett. **20**, 287 (1975).
[3] M. Eschrig, Physics Today **64**, 43 (2011); F. Giazotto and F. Taddei, Phys. Rev. B **77**, 132501 (2008); M. Eschrig, Rep. Prog. Phys. **78**, 104501 (2015).
[4] A.I. Buzdin, L.N. Bulaevskii, S.V. Panyukov, JEPT Lett. **35**, 147 (1982); A.I. Buzdin, Rev. Mod. Phys. **77**, 935 (2005).
[5] F. S. Bergeret, A. F. Volkov, and K. B. Efetov, Phys. Rev. Lett. **86**, 4096 (2001); F. S. Bergeret, K. B. Efetov, and A. I. Larkin, Phys. Rev. B **62**, 11872 (2000); F. S. Bergeret, A. F. Volkov, and K. B. Efetov, Rev. Mod. Phys. **77**, 1321 (2005).
[6] A. Kadigrobov, R. I. Shekhter, and M. Jonson, Europhys. Lett. **54**, 394 (2001).
[7] T. E. Baker, A. Richie-Halford, O. E. Icreverzi, and A. Bill, Europhys. Lett. **107**, 17001 (2014).
[8] T. E. Baker, A. Richie-Halford, and A. Bill, Phys. Rev. B **94**, 104518 (2016).
[9] R. S. Keizer, S. T. B. Goennenwein, T. M. Klapwijk, G. Miao, G. Xiao, and A. Gupta, Nature **439**, 825 (2006).
[10] I. Sosnin, H. Cho, V. T. Petrashov, and A. F. Volkov, Phys. Rev. Lett. **96**, 157002 (2006);
[11] J. W. A. Robinson, J. D. S. Witt, and M. G. Blamire, Science **329**, 59 (2010); G.B. Halász, J.W.A. Robinson, J.F. Annett, and M.G. Blamire, Phys. Rev. B **79**, 224505 (2009); G.B. Halász, M.G. Blamire, and J.W.A. Robinson,Phys. Rev. B **84**, 024517 (2011).
[12] M. S. Anwar, F. Czeschka, M. Hesselberth, M. Porcu, and J. Aarts, Phys. Rev. B **82**, 100501 (2010).
[13] T. S. Khaire, M. A. Khasawneh, W. P. Pratt, Jr., and N. O. Birge, Phys. Rev. Lett. **104**, 137002 (2010); C. Klose, T. S. Khaire, Y. Wang, W. P. Pratt Jr., and N. O. Birge, B. J. McMorran, T. P. Ginley, J. A. Borchers, B. J. Kirby, B. B. Maranville, and J. Unguris, Phys. Rev. Lett. **108**, 127002 (2012); M. A. Khasawneh, T. S. Khaire, C. Klose, W. P. Pratt, Jr., and N. O. Birge, Supercond. Sci. Technol. **24**, 024005 (2011); E. C. Gingrich, P. Quarterman, Y. Wang, R. Loloee, W.P. Pratt Jr, and N.O. Birge, Phys. Rev. B **86**, 224506 (2012).
[14] J. Zhu, I. N. Krivorotov, K. Halterman, and O. T. Valls, Phys. Rev. Lett. **105**, 207002 (2010).
[15] P. V. Leksin, N. N. Garifyanov, I. A. Garifullin, Y. V. Fominov, J. Schumann, Y. Krupskaya, V. Kataev, O. G. Schmidt, and B. Büchner, Phys. Rev. Lett. **109**, 057005 (2012).
[16] L. Wen, L.-J. Jin, Y. Chen, G.-Q. Zha, and S.-P. Zhou, Europhys. Lett. **105**, 27007 (2014).
[17] D. Sprungmann, K. Westerholt, H. Zabel, M. Weides, and H. Kohlstedt, Phys. Rev. B **82**, 060505 (R) (2010).
[18] F. S. Bergeret, A. F. Volkov, and K. B. Efetov, Phys. Rev. B **64**, 134506 (2001);
[19] W. Belzig, F.K. Wilhelm, C. Bruder, and G. Schön, Superlatt. and Microstr. **25**, 1251 (1999).
[20] T. E. Baker, A. Richie-Halford, and A. Bill, New J. Phys. **16**, 093048 (2014)
[21] J. de Rojas, T. E. Baker, A. Richie-Halford, and A. Bill J. of Supercond. Nov. Magn. 25, 2177 (2012).

[22] T. E. Baker and A. Bill, Phys. Rev. B **97**, 214520 (2018).
[23] M. Leadbeater, C. J. Lambert, K. E. Nagaev, R. Raimondi, and A. F. Volkov, Phys. Rev. B **59**, 12264 (1999).
[24] J.-X. Zhu and C. S. Ting, Phys. Rev. **61**, 1456 (1999).
[25] M. Eschrig, T. Löfwander, T. Champel, J. C. Cuevas, J. Kopu, and Gerd Schön, J. Low Temp. Phys. **147**, 457 (2007).
[26] D. Fritsch and J. F. Annett, New J. Phys. **16**, 055005 (2014), *ibid.* J. Phys.: Cond. Mat. **26**, 274212 (2014).
[27] P. G. de Gennes, *Superconductivity of Metals and Alloys*, Addison-Wesley (1989).
[28] K. Halterman and O. T. Valls, Phys. Rev. B **65**, 014509 (2001).
[29] K. Halterman and O. T. Valls, Phys. Rev. B **66**, 224516 (2002).
[30] K. Halterman and O. T. Valls, Phys. Rev. B **70**, 104516 (2004).
[31] K. Halterman and O. T. Valls, Phys. Rev. B **72**, 060514(R).
[32] K. Halterman, P. H. Barsic, and O. T. Valls, Phys. Rev. Lett. **99**, 127002 (2007).
[33] K. Halterman, O. T. Valls, and P. H. Barsic, Phys. Rev. B **77**, 174511 (2008).
[34] Chien-Te Wu, Oriol T. Valls, and Klaus Halterman, Phys. Rev. B **86**, 014523 (2012).
[35] F. S. Bergeret and I. V. Tokatly Phys. Rev. Lett. **110**, 117003 (2013).
[36] A. I. Buzdin and L. N. Bulaevskii, Sov. Phys. JETP **67**, 576 (1988).
[37] P. W. Anderson and H. Suhl, Phys. Rev. **116**, 898 (1959).
[38] G. Annunziata, M. Cuoco, C. Noce, A. Romano, and P. Gentile, Phys. Rev. B **80**, 012503 (2009); G. Annunziata, M. Cuoco, P. Gentile, A. Romano, and C. Noce, Phys. Rev. B **83**, 094507 (2011).
[39] N. Stefanakis and R. Mélin, J. Phys.: Cond. Matter **15**, 3401 (2003).
[40] K. Kuboki and H. Takahashi, Phys. Rev. **70**, 214524 (2004).
[41] L. Covaci and F. Marsiglio, Phys. Rev. B **73**, 014503 (2006).
[42] M. Cuoco, A. Romano, C. Noce and P. Gentile, Phys. Rev. B **78**, 054503 (2008), M. Cuoco, P. Gentile, C. Noce, A. Romano, Z.-J. Ying, and H.-Q. Zhou, J. Phys.: Condens. Matter **21**, 254203 (2009).
[43] G.Q. Zha, L. Covaci, S.P. Zhou and F.M. Peeters, Phys. Rev. B **82**, 140502(R) (2010).
[44] J. E. Hirsch, Phys. Rev. B **40**, 2354 (1989).
[45] J. C. Amadon and J. E. Hirsch, Phys. Rev. B **54**, 6364 (1996).
[46] J. E. Hirsch, Phys. Rev. B **59**, 6256 (1999).
[47] J. E. Hirsch, Phys. Rev. B **59**, 436 (1999).
[48] R. Strack and D. Vollhardt, Phys. Rev. Lett. **72**, 3425 (1994).
[49] H.-Q. Nie and W.-Y. Zhou, Phys. Rev. B **55**, 59 (1997).
[50] M. Kollar and D. Vollhardt, Phys. Rev. B **63**, 045107 (2001).
[51] A. Schiller, Phys. Rev. B **60**, 15660 (1999).
[52] J. E. Hirsch, Phys. Rev. B **44**, 675 (1991).
[53] J. E. Hirsch, Phys. Rev. B **43**, 705 (1991).
[54] A. M. Oles and W. Grzelka, Phys. Rev. B **46**, 5412 (1992).
[55] L. Didukh and O. Kramar, Low Temperature Physics **28**, 30 (2002).
[56] L. Didukh, O. Kramar, and Y. Skorenkyy, Phys. Stat. Sol. (b) **229**, 1241 (2002).
[57] C. Barreteau, M-C. Desjonquères, A. M. Oleś, and D. Spanjaard, Phys. Rev. B **69**, 064432 (2004).
[58] G. Lhoutellier, R. Frésard, and A. M. Oleś, Phys. Rev. B **91**, 224410 (2015).
[59] J. Hubbard, Proc. R. Soc. A **276**, 238 (1963).
[60] J. Kanamori, Prog. Theor. Phys. **30**, 275 (1963).
[61] O. Gunnarsson, Physica B **91**, 329 (1977).
[62] Y. Nagaoka, Phys. Rev. B **147**, 392 (1966); M. Kollar, R. Strack and D. Vollhardt, Phys. Rev. B **53**, 9225 (1996).
[63] E. Dagotto, *Nanoscale Phase Separation and Colossal Magnetoresistance*, Springer (2003).